Formation of Nanocrystalline BiFeO$_3$ under Hydrothermal Conditions

O. V. Proskurina^{a,b}*, M. V. Tomkovich^a, A. K. Bachina^b, V. V. Sokolov^a, D. P. Danilovich^b, V. V. Panchuk^c, V. G. Semenov^c, and V. V. Gusarov^a

^{a} Ioffe Institute, Russian Academy of Sciences,
ul. Politekhnicheskaya 26, St. Petersburg, 194021 Russia
*e-mail: proskurinaov@mail.ru

^{b} St. Petersburg State Institute of Technology (Technical University), St. Petersburg, Russia

^{c} St. Petersburg State University, St. Petersburg, Russia

Abstract—The formation of bismuth orthoferrite under hydrothermal conditions at temperature 160, 180, or 200°C and pressure 100 MPa in aqueous solution of potassium hydroxide has been studied. The determined composition and structure of polycrystalline phase with sillenite structure have evidenced its formation at the interface of the crystallites of amorphous iron oxide. It has been shown that the formation of polycrystalline round-shaped BiFeO$_3$ particles with size about 20 μm occurs via aggregation of perovskite-type phase crystallites (38–70 nm). Pycnometric density of BiFeO$_3$ and the amorphous phase has been determined, and Mossbauer spectra reflecting the state of iron in the phases coexisting during the formation of BiFeO$_3$ have been analyzed.

Keywords: bismuth ferrite, hydrothermal synthesis, Mössbauer spectroscopy, phase formation mechanism

Recently emerged interest in the development and investigation of the materials based on bismuth ferrite with perovskite-type structure is due to their electric, electromechanical, magnetic, magnetoelectric, photo-electric, and photocatalytic properties [1–6]. Importantly, certain special properties of these materials are observed when the crystallite size approaches the nanoscale [7–10].

The importance of the studies of nanomaterials based on BiFeO$_3$ and the complications arising from the demand for the preparation phase-pure materials [11–13] have inspired the development of different synthetic methods [14–19] including the routes to nanocrystalline BiFeO$_3$ [20–24].

Hydrothermal synthesis has been shown promising for the preparation of non-agglomerated nano-crystalline powders of binary and complex oxides with desired morphology and narrow size distribution [25, 26]. Hydrothermal synthesis has been used for the preparation of nanocrystalline BiFeO$_3$ [27–31]. However, not agglomerated nanopowders based on BiFeO$_3$

single-crystal nanoparticles synthesis has faced with a number of problems. For example, BiFeO$_3$ nano-crystals are prone to form aggregates with an irregular shape which are transformed into spherical polycrystalline particles upon prolonged hydrothermal treatment [32–34]. The phase purity of BiFeO$_3$ nanopowders prepared via hydrothermal route is also a prominent issue [35, 36]. Hence, synthesis of nanocrystalline BiFeO$_3$ particles with predefined size and shape demands investigation of the mechanism of their formation under hydrothermal conditions.

Elemental analysis of the samples before and after hydrothermal treatment revealed that the Bi : Fe molar ratio (50.3 : 49.7 and 49.2 : 50.8, respectively) corresponded to the nominal 50: 50 ratio within the limits of the experiment accuracy.

X-ray diffraction patterns of the samples before and after the hydrothermal treatment given in Fig. 1 revealed the significant effect of the treatment temperature on the rate of the formation of BiFeO$_3$. At the same time, the sequence of the processes leading to the

(a)

(b)

(c)
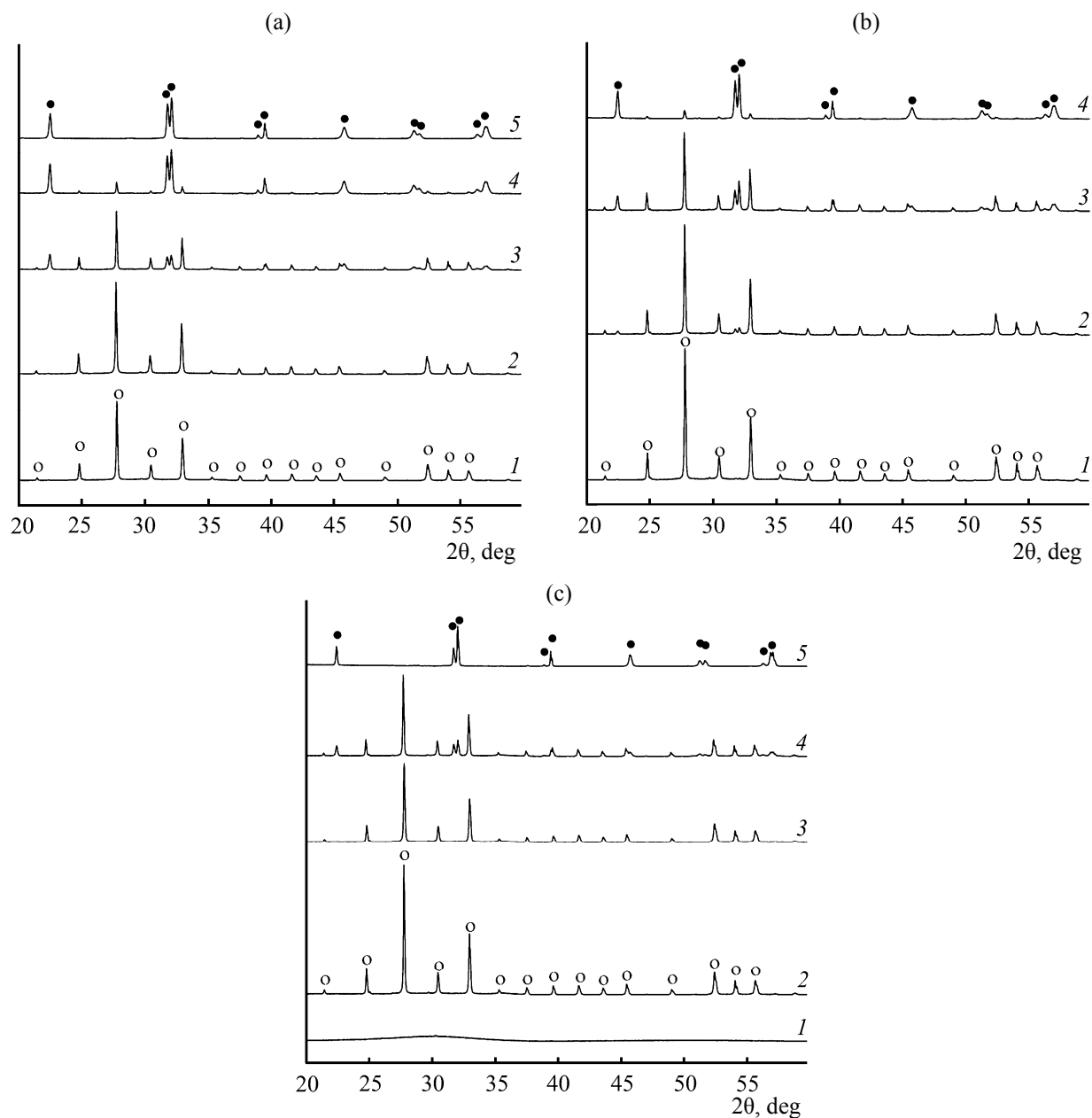
Fig. 1. X-ray diffraction patterns of the starting sample and the samples after hydrothermal treatment at 200 (a), 180 (b), and 160°C (c). The treatment duration, h: (a): (*1*) 0.5, (*2*) 1.5, (*3*) 2.5, (*4*) 3, (*5*) 7; (b): (*1*) 3, (*2*) 5, (*3*) 7, (*4*) 15; (c): (*1*) 0, (*2*) 12, (*3*) 20, (*4*) 22, (*5*) 24. (○) Phase with sillenite structure and (●) $BiFeO_3$.

formation of nanocrystalline $BiFeO_3$ remains the same over the whole temperature range, 160–200°C, under investigation. The first stage consisted in the transformation of X-ray amorphous coprecipitated hydroxides into a substance with sillenite structure, which could be assigned to $Bi_{25}FeO_{39}$ (ICSD code 41937) (Fig. 1). The $BiFeO_3$ was formed in the second stage of hydrothermal synthesis. The X-ray diffraction peaks corresponding to $BiFeO_3$ (ICSD code 163688)

were clearly observed after 22 h of the treatment at 160°C, 5 h at 180°C, and 2 h at 200°C (Fig. 1).

Size distribution and its parameters for crystallites of $Bi_{25}FeO_{39}$ and $BiFeO_3$ after hydrothermal treatment at 200°C and about 100 MPa are shown in Fig. 2. The size distribution of the crystallites with sillenite structure was marginally affected by the treatment duration, except for the shortest treatment (0.25 h), the
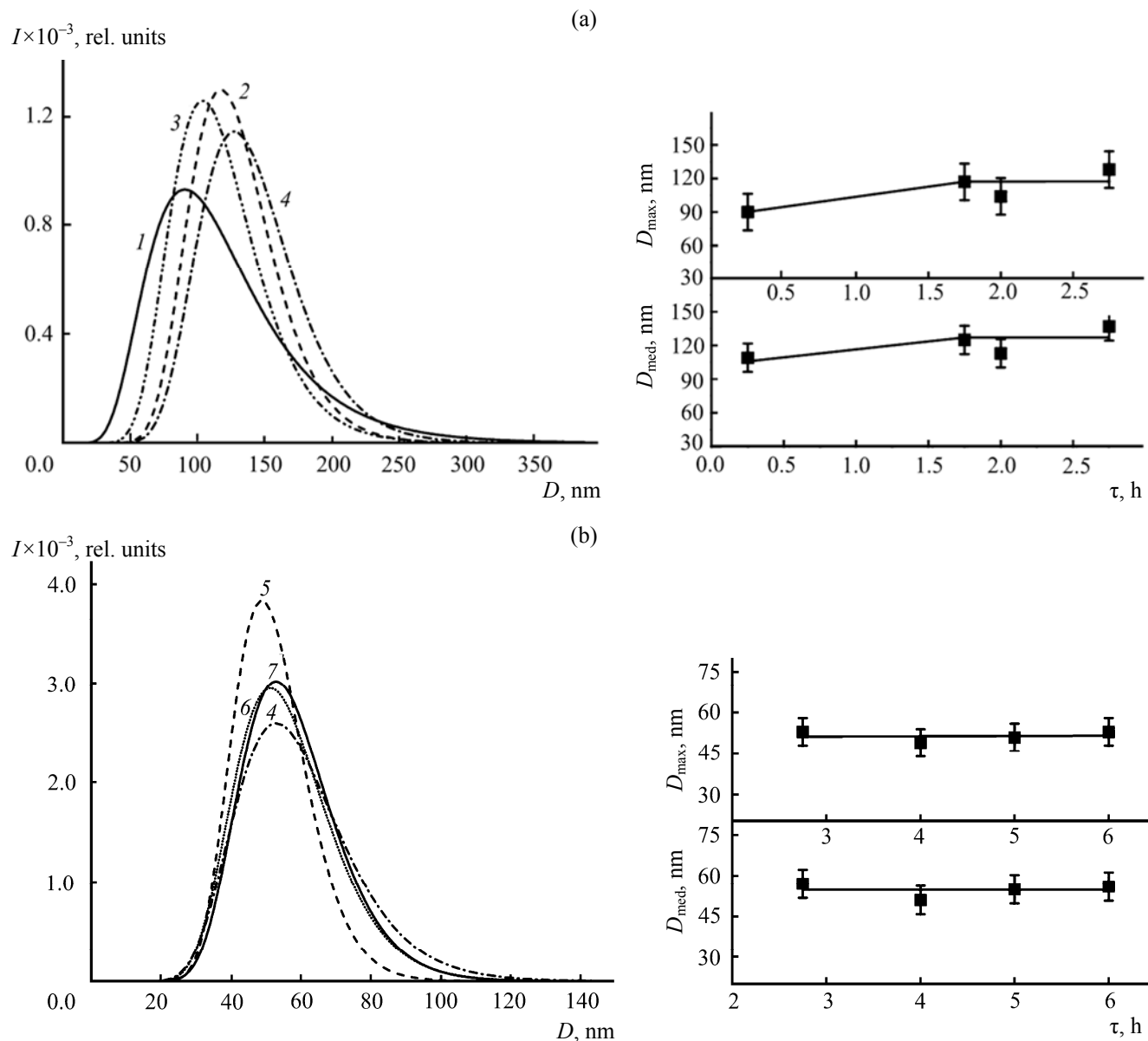
Fig. 2. Size distribution of the crystallites of the phase with sillenite structure (a) and BiFeO$_3$ (b) and size parameters of the crystallites of the corresponding phases depending on the duration of hydrothermal treatment at 200°C: (*1*) 0.25, (*2*) 1.75, (*3*) 2, (*4*) 2.75, (*5*) 4, (*6*) 5, (*7*) 6 h. D_{max} and D_{med} are maximum and median values of the crystallite size.

crystallites being somewhat smaller and more polydisperse in the latter case (Fig. 2). The parameters reflecting size distribution of BiFeO$_3$ crystallites (including the average size) were independent of the hydrothermal treatment duration over the probed time range.

Pycnometric densities of BiFeO$_3$ and the amorphous phase were determined from the data of quantitative X-ray diffraction analysis processed using the density of the phase with sillenite structure calculated from the diffraction data (9.3±0.1 g/cm^3) and

the measured pycnometric density of the samples after the hydrothermal treatment. Pycnometric density was calculated assuming the absence of closed pores in the samples. The phases density was as follows: 8.3±0.1 g/cm^3 for the perovskite-type phase based on BiFeO$_3$ and 2.8±0.5 g/cm^3 for the amorphous phase. It should be noted that the determined pycnometric density of the BiFeO$_3$ phase coincided with its X-ray density (8.314 g/cm^3, ICSD code 163688), thus confirming the assumed absence of the closed pores, at least for the samples consisting majorly of the BiFeO$_3$ phase.
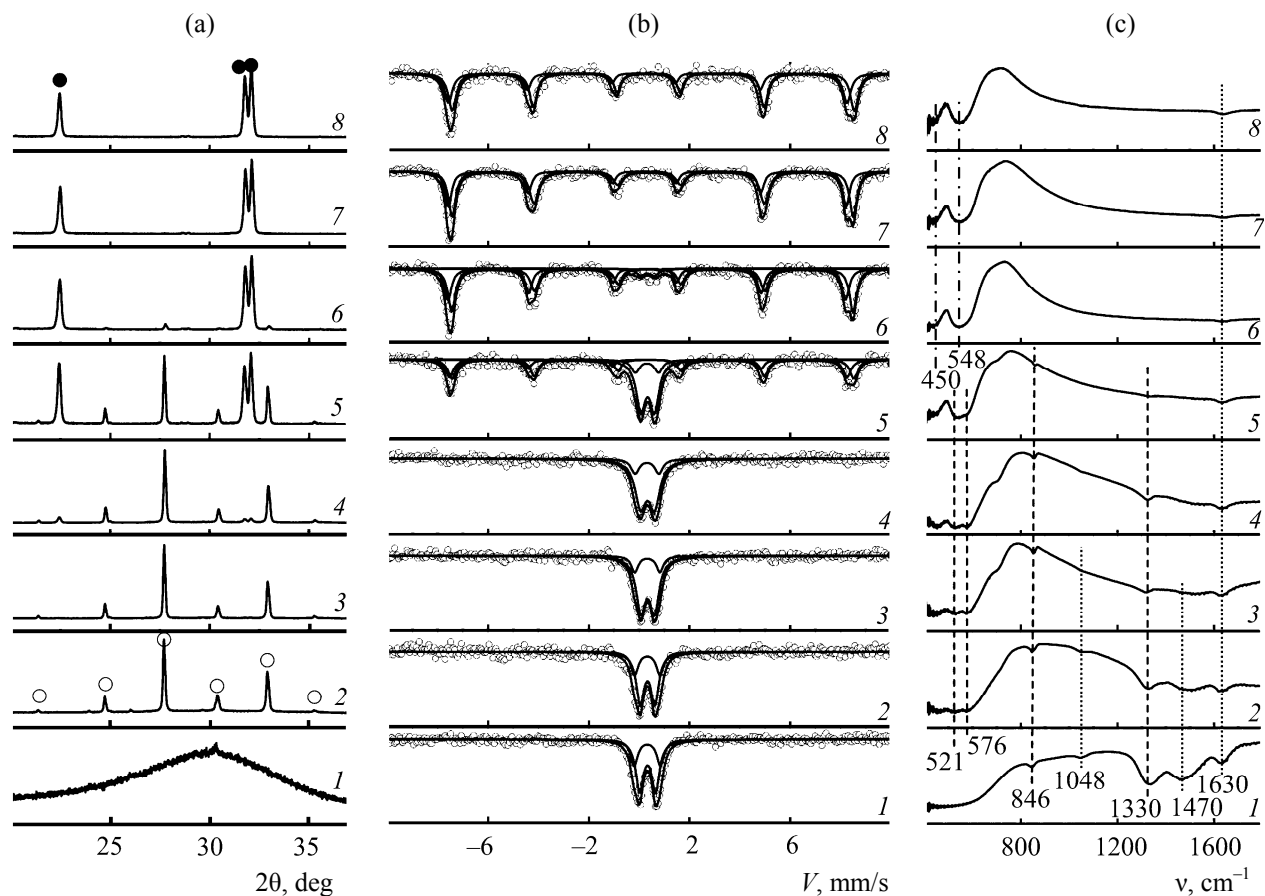
Fig. 3. X-ray diffraction patterns (a), Mössbauer spectra (b), and IR spectra (c) of the starting sample and the samples after hydrothermal treatment at 200°C; the treatment duration, h: (*1*) 0, (*2*) 0.25, (*3*) 1.75, (*4*) 2, (*5*) 2.75, (*6*) 4, (*7*) 5, (*8*) 6 h. (○) Phase with sillenite structure and (●) $BiFeO_3$.

The changes in the Mössbauer spectra of the samples after the hydrothermal treatment at 200°C correlated with the changes in the X-ray diffraction patterns of the samples (Fig. 3). Mössbauer spectra of the starting sample and the sample treated during 2 h could be represented at two superimposed doublets, their parameters remaining unchanged (Fig. 3 and Table 1). X-ray diffraction analysis showed that those samples were majorly X-ray amorphous, containing nanocrystals of $Bi_{25}FeO_{39}$ and traces of nanocrystalline $BiFeO_3$ (after the treatment during 2 h) (Fig. 3). The hydrothermal treatment during 2.75 h or longer resulted in the appearance of additional lines in the Mössbauer spectra, which could be deconvoluted into two sextets with the parameters typical of the magnetically ordered phase (Fig. 3). Comparison of the parameters of sextets (Table 1) with the reference data [37, 38] allowed their assignment to the $BiFeO_3$ phase. The kinetic data on the $BiFeO_3$ formation obtained from Mössbauer spectroscopy and X-ray

diffraction analysis agreed (Fig. 4). At the same time, the diffraction data on the formation of the phase with sillenite structure were not directly confirmed by the Mössbauer spectroscopy, since the spectra did not contain the lines with isomer shift *IS* 0.20± 0.004 mm/s and quadrupole splitting *QS* 0.2±0.07 mm/s assignable to the $Bi_{25}FeO_{39}$ phase [39]. It should be noted that the $Bi_{25}FeO_{39}$ composition of the sillenite-type phase was elucidated from the X-ray diffraction data, whereas the microanalysis revealed the Bi to Fe ratio in that phase ranging between 4 : 1 and 7 : 1 (Fig. 5 and Table 2). The such prominent discrepancy could be explained by partial segregation of iron oxide at the interface of the $Bi_{25}FeO_{39}$ crystallites, since the crystallites with sillenite structure were about 100 nm (Fig. 2), two orders of magnitude smaller than the particles of that phase (about 10 μm, Fig. 5). Let us note that such effect of partial localization of iron oxide at the borders of the crystalline grains has been studied by means of Mössbauer spectroscopy [40, 41];

Table 1. Parameters of Mössbauer spectra

Hydrothermal treatment duration, h	Doublet (D1)		Doublet (D2)		Sextet (S1)			Sextet (S2)		
	IS, mm/s	QS, mm/s	IS, mm/s	QS, mm/s	IS, mm/s	QS, mm/s	H_{eff}, mm/s	IS, mm/s	QS, mm/s	H_{eff}, mm/s
0.00	0.34	0.63	0.32	1.05	–	–	–	–	–	–
0.25	0.33	0.58	0.32	1.01	–	–	–	–	–	–
1.75	0.34	0.54	0.33	1.00	–	–	–	–	–	–
2.00	0.34	0.55	0.31	0.94	–	–	–	–	–	–
2.75	0.34	0.54	0.31	0.92	0.38	−0.33	49.58	0.39	0.05	49.04
4.00	0.34	0.54	0.31	0.92	0.38	−0.30	49.50	0.36	0.11	49.03
5.00	–	–	–	–	0.38	−0.33	49.49	0.36	0.08	49.06
6.00	–	–	–	–	0.38	−0.37	49.59	0.36	0.04	49.15

in these studies, the special state of iron ions was assigned to the doublet of quadrupole splitting with parameters differing from those for iron ions in the crystal.

In this study, we could not detect the state of iron ions in the Bi₂₅FeO₃₉ phase by means of Mössbauer spectroscopy due to the low content of the phase and the low fraction of iron in it. As has been commented in [39], the same reason has led to incorrect assignment [38, 42, 43] of the Bi₂₅FeO₃₉ phase to the doublet with parameters that suggest the state of iron at the intergrain boundaries rather than in the sillenite phase.

Symbate nature of the curves corresponding to D1 doublet and amount of phase with sillenite structure (Fig. 4) demonstrates that the initial X-ray amorphous phase described by D1 doublet and intergrain phase of iron oxide are similar in their structure. Therefore, the decrease in the fraction of the amorphous phase giving rise to the D2 doublet during the first two hours of the hydrothermal treatment at 200°C was due to the transfer of iron oxide to the interface of the nanosized Bi₂₅FeO₃₉ crystallites forming polycrystalline grains of the phase with the sillenite structure. Further decrease in the fraction of the X-ray amorphous phase with the state of iron oxide characterized by doublets D1 and D2 was determined by the formation of BiFeO₃ particles (Fig. 4). Certain difference in the contents of the BiFeO₃ phase determined by means of X-ray diffraction and Mössbauer spectroscopy was due to the assumptions used in the calculations.

Figure 3c displays the IR spectra of the samples differing in the hydrothermal treatment duration. The bands at 521, 576, 846, and 1330 cm⁻¹ were assigned

to the metal–oxygen bonds vibrations in the phase with sillenite structure [35, 44]. The bands at 450 and 548 cm⁻¹ could be assigned to stretching and deformation of octahedral elements of perovskite [35, 44]. The band at 1630 cm⁻¹ was assigned to deformation vibrations of H₂O molecule [27, 35], whereas the bands at 1048 and 1470 cm⁻¹ corresponded to deformation vibrations of the OH group in FeOOH [45].

Certain similarity in the IR spectra of the X-ray amorphous phase and the phase with sillenite structure (Fig. 3) suggested the similar structure of the first coordination sphere in sillenite and some pre-nucleus clusters in the amorphous phase. Likely, that resulted
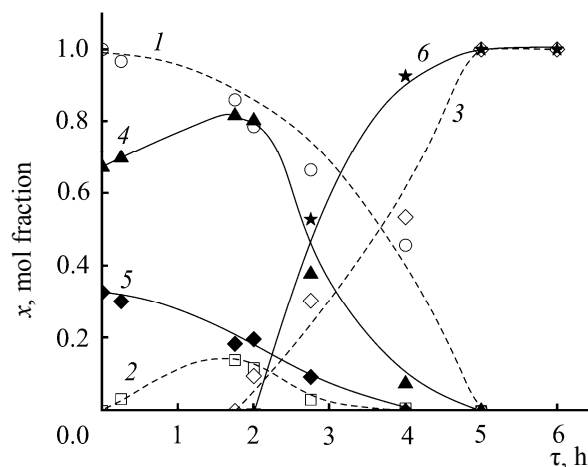
Fig. 4. Evolution of the phase composition of the samples during hydrothermal treatment at 200°C according to X-ray diffraction data (dashed lines) and Mössbauer spectroscopy (solid lines): (*1*) amorphous substance; (*2*) phase with sillenite structure; (*3*) BiFeO₃; (*4*) doublet D1; (*5*) doublet D2; (*6*) sum of sextets (S1 and S2).

(a)

(b)

(c)

(d)
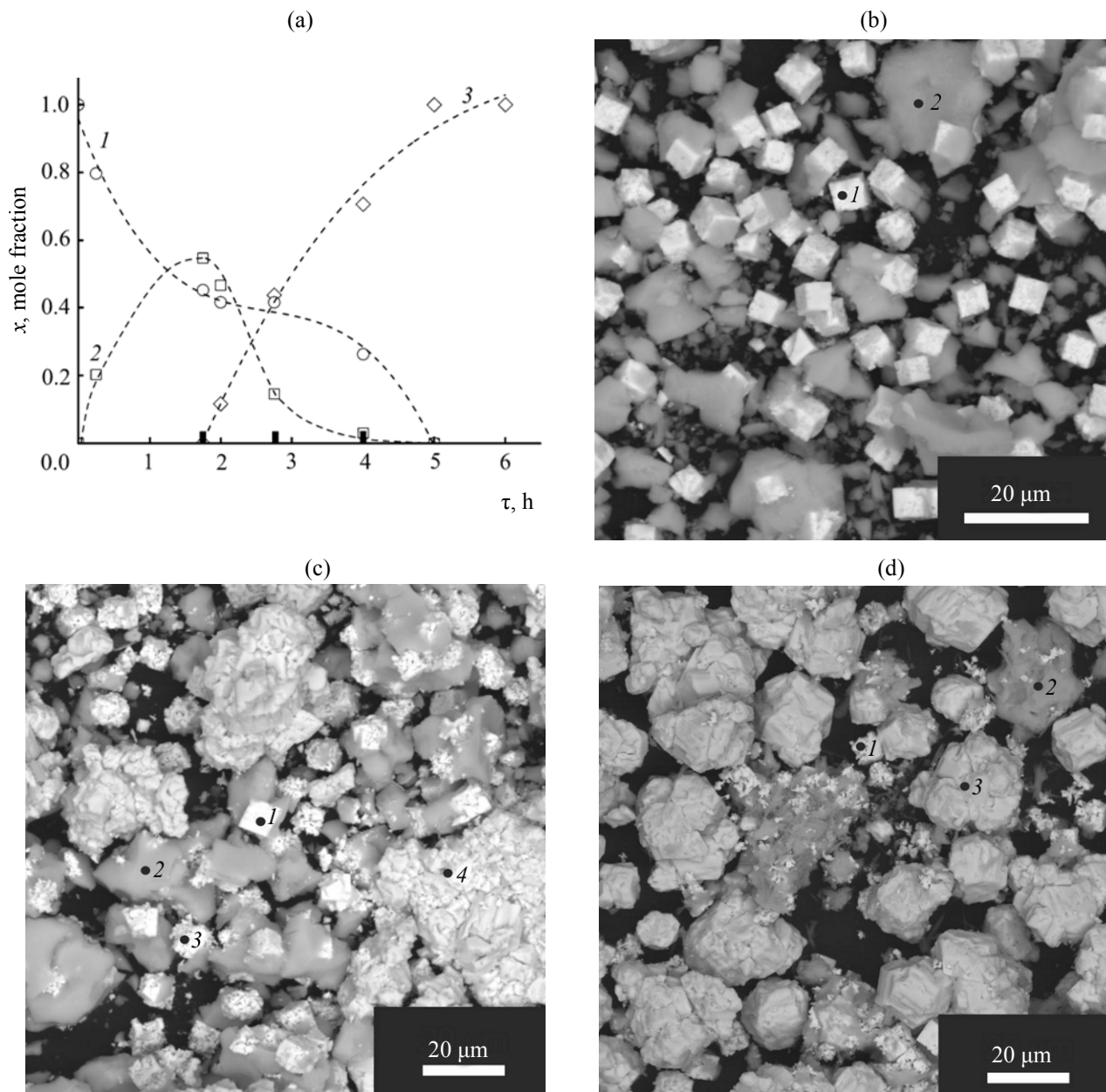
Fig. 5. Volume fraction of the coexisting phases as a function of the duration of hydrothermal treatment at 200°C (a) and microscopy images of the samples treated during 1.75 (b), 2.75 (c), and 4 h (d): (*1*) amorphous substance, (*2*) phase with sillenite structure, (*3*) BiFeO$_3$.

in the formation of Bi$_{25}$FeO$_{39}$ nanocrystals after short hydrothermal treatment. It should be noted that the same reason could explain the formation of the particles with sillenite structure at relatively low-temperature hydrothermal treatment (160°C, Fig. 1) and even under ambient conditions [39].

Comparison of the data of IR spectroscopy, X-ray diffraction, Mössbauer spectroscopy, electron micro-

scopy, and elemental microanalysis suggested the following mechanism of the formation of the phase with sillenite structure. First, 100 nm nanocrystals with sillenite structure and relatively narrow size distribution were formed from the pre-nucleus clusters. Those crystallites aggregated [46] into about 10 μm cubic crystals with certain amount of intergrain phase based on iron oxide crystallized at their interface. The boundary X-ray amorphous area was enriched in iron

Table 2. Phase state and elemental composition of the selected samples areas

Hydrothermal treatment duration, h	Area[a]	Fe : Bi, mol %		Structure state
		Fe	Bi	
1.75	1	20.5	79.5	Sillenite
	2	77.5	22.5	Amorphous phase
2.75	1	14.5	85.5	Sillenite
	2	81.9	18.1	Amorphous phase
	3	19.0	81.0	Sillenite
	4	51.5	48.5	Perovskite
4.00	1	12.0	88.0	Sillenite
	2	89.9	10.1	Amorphous phase
	3	49.8	50.2	Perovskite

[a] The area for the elemental composition determination is shown in Fig. 5.

oxide preventing the formation of crystallites based on Bi$_{25}$FeO$_{39}$.

When the possibilities of the formation of the phase with sillenite structure at the interphase between the Fe$_2$O$_3$-enriched amorphous phase and the hydrothermal fluid were exhausted, the BiFeO$_3$ nanocrystals were formed. Since the formation of BiFeO$_3$ particles was determined by the transfer of one of the components at the interphase boundary thus enriched with bismuth oxide and iron oxide, the increase in the BiFeO$_3$ content was due to the nucleation at the interface rather than the nuclei growth; indeed, the increase in the BiFeO$_3$ fraction in the system (Fig. 4) was not accompanied by the increase in its crystallites size (50 nm over the probed process duration range, Fig. 2). The BiFeO$_3$ particles grew via the aggregation mechanism [46] forming the polycrystalline objects (Fig. 5), similarly to the phase with sillenite structure.

It should be noted that the suggested mechanism of BiFeO$_3$ formation explains the appearance of polycrystalline aggregates from the BiFeO$_3$ nanocrystals observed in this study as well as in other studies using the same method of synthesis [32–34].

EXPERIMENTAL

Bi(NO$_3$)$_3$·5H$_2$O ("special pure" grade), Fe(NO$_3$)$_3$·9H$_2$O ("pure" grade), 6 mol/L aqueous solution of nitric acid ("special pure" grade), and 4 mol/L aqueous solution of KOH ("analytical pure" grade) were used as the starting components.

Bismuth nitrate (the amount required for the preparation of 1 g of BiFeO$_3$) was dissolved at heating in 2 mL of 6 mol/L nitric acid. Iron nitrate was added at stirring, the Bi : Fe ratio being 1 : 1. The solution was stirred during 30 min, and then added dropwise to 20 mL of 4 mol/L KOH at stirring and ultrasonication (submersible dispenser VENPAN UD-20). Coprecipitation of hydroxides was performed over 1–1.5 min, and then the formed precipitate was centrifuged off and washed either with distilled water (to obtain the starting sample) or with 4 mol/L KOH (to be used in hydrothermal synthesis).

Hydrothermal treatment was performed in 4 mol/L aqueous KOH using stainless steel reactors with Teflon reaction vessel (volume 25 mL, temperature 160, 180, or 200°C, and pressure 100 MPa). The Teflon vessel with the precipitate was put in the pre-heated reactor, quickly closed, and left in an oven for the desired synthesis duration. After the isothermal heating, the reactor was cooled to 50°C during 10 min. The precipitate was centrifuged off, washed with water, and dried at 70°C for 12 h.

Morphology and size of the particles and elemental composition of the samples (overall as well as local) were determined using a Tescan Vega 3 SBH scanning electron microscope equipped with an X-ray spectral microanalysis attachment (Oxford Instruments).

X-ray diffraction patterns were obtained using a Rigaku SmartLab 3 diffractometer (CuK_α, 2θ 20°–60° with 0.01° spacing). Phase composition of the samples was elucidated using the ICSD PDF-2 database. Quantitative X-ray diffraction analysis was performed using α-Al_2O_3 as the internal reference. The mass fractions were recalculated in molar and volume fractions using the elemental composition determined by means of X-ray spectral microanalysis and the data on the pycnometric density of the phases. The size distribu-tion of crystallites and the distribution parameters were determined using the method of fundamental param-eters implemented in SmartLab Studio II software package (Rigaku).

Mössbauer spectroscopy studies were performed using a Wissel GmbH multifunctional Mössbauer spectrometer in the constant acceleration mode at room temperature. Co-57 in Rh matrix (activity 30 mCi) was used as the source. The isomer shift was determined with respect to α-Fe. Statistical analysis of the spectra was performed using DISTR routine of MSTools software package [47]. Relative fractions of iron in different states were determined from the data on integral intensities of the corresponding lines in the spectra assuming closeness of the Mössbauer coefficients for those states.

IR spectra were recorded using a FSM 1202 Fourier spectrometer. Pycnometric density was determined using a Quantachrome Ultrapycnometer 1000 helium pycnometer.

X-ray diffraction, scanning electron microscopy, and elemental analysis studies were performed using the equipment of Engineering Center of St. Petersburg State Institute of Technology (Technical University).

ACKNOWLEDGMENTS

REFERENCES

1. Rojac, T., Bencan, A., Malic, B., Tutuncu, G., Jones, J.L., Daniels, J.E., and Damjanovic, D., *J. Am. Ceram. Soc.*, 2014, vol. 97, no. 7, p. 1993. doi 10.1111/jace.12982

2. Lin, Z., Cai, W., Jiang, W., Fu Ch., Li Ch., and Song, Y., *Ceram. Intern.*, 2013, vol. 39, p. 8729. doi 10.1016/j.ceramint.2013.04.058

3. Selbach, S.M., Tybell, T., Einarsrud, M.A., and Grande, T., *Chem. Mat.*, 2007, vol. 19, p. 6478. doi 10.1016/j.jssc.2010.03.014

4. Shirokov, V.B. Golovko, Yu.I., and Mukhortov, V.M., *Techn. Phys.*, 2014, vol. 59, no. 1, p. 102. doi 10.1134/S1063784214010174

5. Dziubaniuka, M., Bujakiewicz-Koronska, R., Sucha-nicz, J., Wyrwaa, J., and Rekas, M., *Sensors and Actuators (B)*, 2013, vol. 188, p. 957. doi 10.1016/j.snb.2013.08.020

6. Golić, D.L., Radojković, A., Ćirković, J., Dapčević, A., Pajić, D., Tasić, N., Savić, S.M., Počuča-Nešić, M., Marković, S., Branković, G., Stanojević, Z.M., and Branković, Z., *J. Eur. Ceram. Soc.*, 2016, vol. 36, no. 7, p. 1623. doi 10.1016/j.jeurceramsoc.2016.01.031

7. Srivastav, S.K., Johari, A., Patel, S.K.S., and Gajbhiye, N.S., *J. Magn. Magn. Mater.*, 2017, vol. 441, p. 503. doi 10.1016/j.jmmm.2017.06.025

8. Hengky Ch., Moya, X., Mathurc, N.D., and Dunn, S., *RSC Adv.*, 2012, vol. 2, p. 11843. doi 10.1039/c2ra22211f

9. Du, Y., Cheng, Z.X., Dou, S.X., Attard, D.J., and Wang, X.L., *J. Appl. Phys.*, 2011, vol. 109, p. 073903. doi 10.1063/1.3561377

10. Ortiz-Quinones, J.L., Diaz, D., Zumeta-Dube, I., Arriola-Santamaria, H., Betancourt, I., Santiago-Jacinto, P., and Nava-Etzana, N., *Inorg. Chem.*, 2013, vol. 52, p. 10306. doi 10.1021/ic400627c

11. Morozov, M.I., Lomanova, N.A., and Gusarov, V.V., *Russ. J. Gen. Chem.*, 2003, vol. 73, no. 11, p. 1676. doi 10.1023/B:RUGC.0000018640.30953.70

12. Liu, T., Xu, Y., and Zhao, J., *J. Am. Ceram. Soc.*, 2010, vol. 93, no. 11, p. 3637. doi 10.1111/j.1551-2916.2010.03945.x

13. Feroze, A., Idrees, M., Kim, D.-K., Nadeem, M., Siddiqi, S.A., Shaukat, S.F., Atif, M., and Siddique, M., *J. Electron. Mater.*, 2017. doi 10.1007/s11664-017-5463-3

14. Selbach, S.M., Einarsrud, M., Tybell, T., and Grande, T., *J. Am. Ceram. Soc.*, 2007, vol. 90, no. 11, p. 3430. doi 10.1111/j.1551-2916.2007.01937.x

15. Chen, J., Xing, X., Watson, A., Wang, W., Yu, R., Deng, J., Yan, L., Sun, C., and Chen, X., *Chem. Mater.*, 2006, vol. 19, no. 15, p. 3598. doi 10.1021/cm070790c

16. Kothai, V. and Rajeev, R., *Bull. Mat. Sci.*, 2012, vol. 35, no. 2, p. 157. doi 10.1007/s12034-012-0266-x

17. Lomanova, N.A., Tomkovich, M.V., Sokolov, V.V., and Gusarov, V.V., *Russ. J. Gen. Chem.*, 2016, vol. 86, no. 10, p. 2256. doi 10.1134/S1070363216100030

18. Suresh, P. and Srinath, S*., J. Alloys Compd.*, 2015, vol. 649, p. 843. doi 10.1016/j.jallcom.2015.07.152

19. Sakar, M., Balakumar, S., Saravanan, P., and Jaisankar, S., *Mater. Res. Bull.*, 2013, vol. 48, no. 8, p. 2878. doi 10.1016/j.materresbull.2013.04.008

20. Wei, J. and Xue, D., *Mater. Res. Bull.*, 2008, vol. 43, p. 3368. doi 10.1016/j.materresbull.2008.02.009

21. Chaudhuri, A., Mitra, S., Mandal, M., and Mandal, K., *J. Alloys Compd.*, 2010, vol. 491, p. 703. doi 10.1016/j.jallcom.2009. 11.049

22. Zhang, Q., Sando, D., and Nagarajan, V., *J. Mater. Chem. (C)*, 2016, vol. 4, p. 4092. doi 10.1039/C6TC00243A

23. Zou, J., Gong, W., Ma, J., Li, L., and Jiang, J., *J. Nanosci. Nanotechnol.*, 2015, vol. 15, p. 1304. doi 10.1166/jnn.2015.9074

24. Guo, Y., Pu, Y., Cui, Y., Hui, C., Wan, J., and Cui, C., *Mater. Lett.*, 2017, vol. 196, p. 57. doi 10.1016/j.matlet.2017.03.023

25. Pozhidaeva, O.V., Korytkova, E.N., Romanov, D.P., and Gusarov, V.V., *Russ. J. Gen. Chem.*, 2002, vol. 72, no. 6, p. 849. doi 10.1023/A:1020409702215

26. Almjasheva, O.V., *Nanosystems: Physics, Chemistry, Mathematics*, 2016, vol. 7, no. 6, p. 1031. doi 10.17586/2220-8054-2016-7-6-1031-1049

27. Čebela, M., Janković, B., Hercigonja, R., Lukić, M.J., Dohčević-Mitrović, Z., Milivojević, D., and Matović, B., *Proc. Appl. Ceram.*, 2016, vol. 10, no. 4, p. 201. doi 10.2298/PAC1604201C

28. Wang, X., Mao, W., Zhang, Q., Wang, Q., Zhu, Y., Zhang, J., Yang, T., Yang, J., Li, X., and Huang, W., *J. Alloys Compd.*, 2016, vol. 677, p. 288. doi 10.1016/j.jallcom.2016.02.246

29. Niu, F., Gao, T., Zhang, N., Chen, Z., Huang, Q., Qin, L., Sun, X., and Huang, Y., *J. Nanosci. Nanotechnol.*, 2015, vol. 15, p. 9693. doi 10.1166/jnn.2015.10682

30. Di, L.J., Yang, H., Xian, T., Li, R.S., Feng, Y.C., and Feng, W.J., *Ceramics Int.*, 2014, vol. 40, no. 1, p. 4575. doi 10.1016/j.ceramint., 2013.08.134

31. Shun, L., Nechache, R., Davalos, I.A.V., Goupil, G., Nikolova, L., Nicklaus, M., Laverdiere, J., Ruediger, A., and Rosei, F., *J. Am. Ceram. Soc.*, 2013, vol. 96, no. 10, p. 3155. doi 10.1111/jace. 12473

32. Chybczynska, K., Blaszyk, M., Hilczer, B., Lucinski, T., Matczak, M., and Andrzejewski, B., *Mater. Res. Bull.*, 2017, vol. 86, p. 178. doi 10.1016/j.materresbull.2016.10.024

33. Suzuki, K., Tokudome, Y., Tsuda, H., and Takahashi, M., *J. Appl. Crystallogr.*, 2016, vol. 49, no. 1, p. 168. doi 10.1107/S1600576715023845

34. Xu, X., Xu, Q., Huang, Y., Hu, X., Huang, Y., Wang, G., Hun, X., and Zhuang, N., *J. Crystal Growth.*, 2016, vol. 437, p. 42. doi 10.1016/j.jcrysgro.2015.12.015

35. Cao, W., Chen, Z., Gao, T., Zhou, D., Leng, X., Niu, F., Zhu, Y., Qin, L., Wang, J., and Huang, Y., *Mater. Chem. Phys.*, 2016, vol. 175, p. 1. doi 10.1016/j.matchemphys.2016.02.067

36. Chen, Z. and Jin, W., *J. Mater. Sci.*, 2014, vol. 25, no. 9, p. 4039. doi 10.1007/s10854-014-2126-5

37. Jartych, E., Oleszak, D., and Mazurek, M., *Przeglad Elektrotechniczny* (Electrical Review), 2012, no. 9b, p. 242.

38. Jartych, E., Lisinska-Czekaj, A., Oleszak, D., and Czekaj, D., *Materials Science-Poland.,* 2013, vol. 31, no. 2, p. 211. doi 10.2478/s13536-012-0093-1

39. Flores Morales, S.S., León Flores, J.A., Pérez Mazariego, J.L., Marquina Fábrega, V., and Gómez González, R.W., *Physica (B)*, 2017, vol. 504, p. 109. doi 10.1016/j.physb.2016.10.019

40. Gusarov, V.V., Egorov, F.K., Ekimov, S.P., and Suvorov, S.A., *Zh. Fiz. Khim.*, 1987, vol. 61, no. 6, p. 1652.

41. Gusarov, V.V., Malkov, A.A., Malygin, A.A., and Suvorov, S.A., *Inorg. Mater.*, 1995, vol. 31, no. 3, p. 320.

42. Ncube, M., Naidoo, D., Bharuth-Ram, K., Billing, D., Masenda, H., Sahu, D.R., Roul, B.K., and Erasmus, R.M., *Hyperfine Interact.*, 2013, vol. 219, p. 83. doi 10.1007/s10751-012-0729-x

43. Santos, I.A., Grande, H.L.C., Freitas, V.F., de Medeiros, S.N., Paesano Jr, A., Cótica, L.F., and Radovanovic, E., *J. Non-Cryst. Solids*, 2006, vol. 352, p. 3721. doi 10.1016/j.jnoncrysol.2006. 02.122

44. Vasconcelos, I.F., Pimenta, M.A., and Sombra, A.S.B., *J. Mater. Sci.*, 2001, vol. 36, no. 3, p. 587. doi 10.1023/A:1004804000723

45. Musić, S., Czakó-Nagy, I., Popović, S., Vértes, A., and Tonković, M., *Croat. Chem. Acta*, 1986, vol. 59, no. 4, p. 833.

46. Ivanov, V.K., Fedorov, P.P., Baranchikov, A.Y., and Osiko, V.V., *Russ. Chem. Rev.*, 2014, vol. 83, no. 12, p. 1204. doi 10.1070/RCR4453

47. Rusakov, V.S. and Kadyrzhanov, K.K., *Hyperfine Interact.*, 2005, vol. 164, p. 87. doi 10.1007/s10751-006-9236-2